JACS
JOURNAL OF THE AMERICAN CHEMICAL SOCIETY
Article
pubs.acs.org/JACS

Low Overpotential in Vacancy-Rich Ultrathin $CoSe_2$ Nanosheets for Water Oxidation

Youwen Liu,[†,∥] Hao Cheng,[‡,∥] Mengjie Lyu,[†] Shaojuan Fan,[§] Qinghua Liu,[‡] Wenshuai Zhang,[§] Yuduo Zhi,[†] Chengming Wang,[†] Chong Xiao,*[,†] Shiqiang Wei,*[,‡] Bangjiao Ye,[§] and Yi Xie*[,†]

[†]Hefei National Laboratory for Physical Sciences at the Microscale, University of Science & Technology of China, Hefei, Anhui 230026, People's Republic of China

[‡]National Synchrotron Radiation Laboratory, University of Science & Technology of China. Hefei, Anhui 230029, People's Republic of China

[§]State Key Laboratory of Particle Detection and Electronics, University of Science & Technology of China, Hefei, Anhui 230026, People's Republic of China

Supporting Information

ABSTRACT: According to Yang Shao-Horn's principle, $CoSe_2$ is a promising candidate as an efficient, affordable, and sustainable alternative electrocatalyst for the oxygen evolution reaction, owing to its well-suited electronic configuration of Co ions. However, the catalytic efficiency of pure $CoSe_2$ is still far below what is expected, because of its poor active site exposure yield. Herein, we successfully overcome the disadvantage of insufficient active sites in bulk $CoSe_2$ by reducing its thickness into the atomic scale rather than any additional modification (such as doping or hybridizing with graphene or noble metals). The positron annihilation spectrometry and XAFS spectra provide clear evidence that a large number of V_{Co}'' vacancies formed in the ultrathin nanosheets. The first-principles calculations reveal that these V_{Co}'' vacancies can serve as active sites to efficiently catalyze the oxygen evolution reaction, manifesting an OER overpotential as low as 0.32 V at 10 mA cm^{-2} in pH 13 medium, which is superior to the values for its bulk counterparts as well as those for the most reported Co-based electrocatalysts. Considering the outstanding performance of the simple, unmodified ultrathin $CoSe_2$ nanosheets as the only catalyst, further improvement of the catalytic activity is expected when various strategies of doping or hybridizing are used. These results not only demonstrate the potential of a notable, affordable, and earth-abundant water oxidation electrocatalyst based on ultrathin $CoSe_2$ nanosheets but also open up a promising avenue into the exploration of excellent active and durable catalysts toward replacing noble metals for oxygen electrocatalysis.

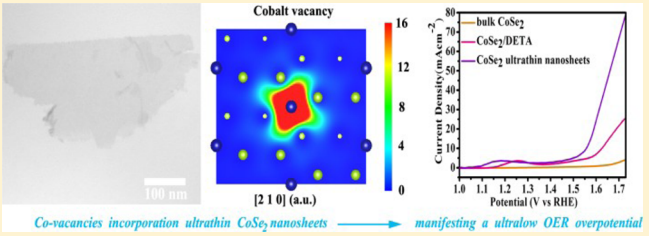

INTRODUCTION

As the key enabling process in various types of clean and sustainable energy technologies, electrochemical water oxidation, also known as the oxygen evolution reaction (OER), has stimulated extensive research in the societal pursuit of efficient energy storage and conversion.[1−4] However, the kinetics of the OER are sluggish, which requires a high overpotential to experience a complex four-electron oxidation process.[5,6] Although pioneering studies have revealed that some noble metal oxides, such as IrO_2 and RuO_2, can efficiently catalyze the OER process, their prohibitive cost and scarcity have seriously impeded their widespread application.[7,8] Therefore, the exploration of highly efficient and economical water oxidation catalysts has became more significant in light of the dwindling global energy crisis and environmental challenges.

Recently, 3d transition metal (Ni, Co, Fe, and Mn) compounds have sparked worldwide interest owing to the fact that they are earth-abundant and environmentally benign; however, they underperform the state-of-the-art water oxidation catalysts.[9−13] Yang Shao-Horn's principle, which quantificationally describes that the ideal OER electrocatalyst can be obtained when the e_g occupancy of surface transition-metal cations is close to unity, has been instrumental in designing highly active water oxidation catalysts.[14] In this regard, cubic $CoSe_2$, with a $t_{2g}^6e_g^1$ electronic configuration near the optimal e_g filling (Figure 1a,b), would be a terrific candidate. Meanwhile, theoretical calculations show the large local density of states (DOS) across the Fermi level (Figure 1c), which reveals the metallic behavior in $CoSe_2$. To confirm the theoretical investigations, the temperature dependence of the resistance was measured further. As shown in Figure 1d, the typical metallic behavior of $CoSe_2$ is reflected by the increased electrical resistance as the temperature increases, which ensures the efficient migration of electrons between the electrode and the surface of the catalysts to give high-performance OER

Received: August 19, 2014
Published: October 13, 2014

   dx.doi.org/10.1021/ja5085157 | J. Am. Chem. Soc. 2014, 136, 15670−15675

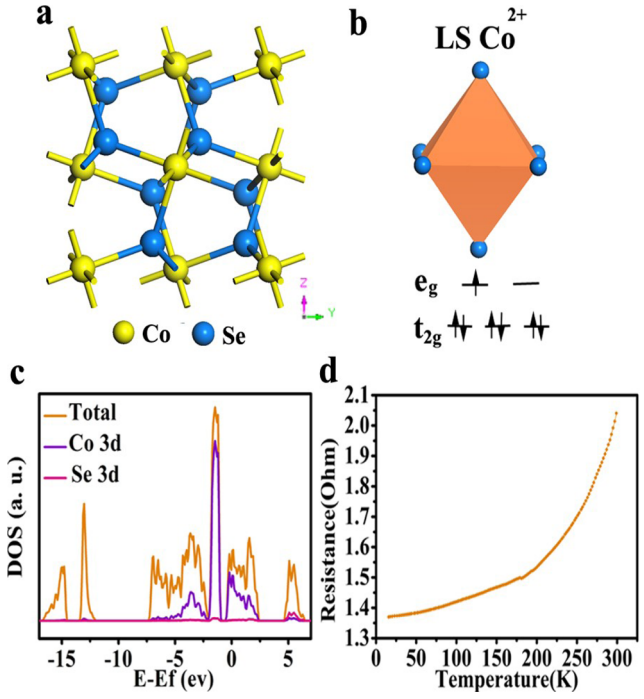

Figure 1. Crystal structure, DOS diagram, and temperature dependence of resistance: (a) crystal structure of $CoSe_2$ in the cubic pyrite-type phase; (b) schematic spin structure of the Co cation; (c) DOS diagram for $CoSe_2$; (d) temperature dependence of bulk $CoSe_2$ resistance.

catalysts. With these facts in mind, $CoSe_2$ would enable tremendous advances in high-performance OER. However, despite its optimal e_g filling, pure $CoSe_2$ still exhibits relatively low catalytic activity, due to its poor active site exposure yield. Although a significant number of strategies, such as hybridizing with graphene or noble metals, have been used to improve the OER catalysis performance of $CoSe_2$,[15−17] a systematic investigation of electrocatalysis of pure $CoSe_2$ has long been neglected, leading to the fact that its catalytic efficiency is still far below what is expected. Therefore, it is highly desirable and urgent to develop a new and convenient strategy to overcome those disadvantages to achieve the excellent intrinsic electrocatalytic activity of this promising compound.

Triggered by the great success of graphene, two-dimensional (2D) ultrathin nanosheets have attracted explosive attention due to a wealth of unprecedented functionalities, which benefit from their extremely high surface percentage (nearly 100%).[18−22] Moreover, ultrathin nanosheets with 2D configurations enable intimate and large area contact with both the GC electrode and the electrolyte, which guarantee faster interfacial charge transfer to improve the electrocatalytic reactions.[23] Most importantly, the more exposed interior atoms inevitably induce the formation of defects with structure disorder on their surface,[24] which usually increases the density of states near the Fermi level to serve as highly active sites for catalytic reactions. Thus, 2D ultrathin nanosheets undoubtedly provide not only new opportunities to satisfy the requirements of highly efficient catalysts but also an ideal platform for a comprehensive understanding of the underlying correlations among atomic, defect, electronic structure, and intrinsic properties.

Herein, inspired by the above considerations, we show that the atomically thick $CoSe_2$ nanosheets can effectively catalyze the OER without any additional modification (such as doping or hybridizing with graphene or noble metals), manifesting an OER overpotential as low as 0.32 V at a current density of 10 mA cm^{-2} in pH 13 medium, which is almost the best performance among the reported Co-based OER electrocatalysts. These ultrathin $CoSe_2$ nanosheets also show small Tafel slopes of 44 mV/dec and large turnover frequencies (TOFs) of 0.33 s^{-1} at an overpotential of 0.5 V, which indicates that the ultrathin nanosheets should be promising candidates for highly active electrocatalysts. In combination with positron annihilation spectra, XAFS spectra, and theoretical calculations, we can unambiguously conclude that the formation of V_{Co}'' vacancies in the two-dimensional plane should mainly contribute to the significantly improved OER catalytic performance. Our work undoubtedly provides prospective insights into the exploration of highly efficient and durable electrocatalysts for water oxidation.

EXPERIMENTAL SECTION

Materials. $Co(AC)_2{\cdot}H_2O$, K_2SeO_3, diethylenetriamine (DETA), cobalt powder, selenium powder, ethanol, KOH, and Nafion solution (5 wt %) were all analytical grade purity acquired from Sinopharm Chemical Reagent Co., Ltd. and were used without any further purification.

Synthesis of Nanohybrids, $CoSe_2$ Ultrathin Nanosheets, and Bulk $CoSe_2$. $CoSe_2$ ultrathin nanosheets were fabricated by exfoliating the $CoSe_2$-based inorganic−organic lamellar nanohybrids. The typical experiment was mainly divided into two steps: first, lamellar hybrid $CoSe_2$/DETA intermediates were synthesized in conformity to the existing literature.[25] Herein, DETA in the intermediates $CoSe_2$/DETA stands for diethylenetriamine. Second, 10 mg of $CoSe_2$/DETA product was dispersed in 20 mL of ethanol and then ultrasonicated in ice−water for 12 h. After ultrasonic treatment, the resultant dispersions were centrifuged at 3000 rpm for 10 min to remove the unexfoliated component. The bulk $CoSe_2$ was synthesized by solid-state reactions. Typically, the cobalt powder and selenium powder mixture in a stoichiometric ratio was ground and then collected in a fused silica tube under vacuum, which was heated to 500 °C for 2 h at a rate of 50 °C h^{-1} and then heated at the same rate to 650 °C. After sintering at 650 °C for 12 h, the obtained samples were cooled to room temperature over 12 h.

Characterization. XRD patterns were recorded by using a Philips X'Pert Pro Super diffractometer with Cu Kα radiation (λ = 1.54178 Å). Raman spectra were detected by a Renishaw RM3000 Micro-Raman system. X-ray photoelectron spectroscopy (XPS) measurements were performed on a VGESCALAB MK II X-ray photoelectron spectrometer with an excitation source of Mg Kα (1253.6 eV). Thermogravimetric analysis (TGA) was carried out on a Shimadzu TA-50 thermal analyzer from room temperature to 800 °C at a heating rate of 10 °C min^{-1}. The field emission scanning electron microscopy (FE-SEM) images were taken on a JEOL JSM-6700F SEM instrument. The TEM and HRTEM measurements were carried out on a JEM-2100F field emission electron microscope at an acceleration voltage of 200 kV. Atomic force microscopy (AFM) was performed by means of a DI Innova Multimode SPM platform. The electrical resistivity study in this work was corrected for a Keithley 4200 station with the computer-controlled four-probe technique. Co K-edge X-ray absorption fine structure spectroscopy (XAFS) was carried out at the BL14W1 beamline of the Shanghai Synchrotron Radiation Facility (SSRF) China. The storage ring of the SSRF was operated at 3.5 GeV with a maximum current of 200 mA.

Positron Annihilation Measurement. Sandwiched samples of $CoSe_2$/^{22}Na source/$CoSe_2$ with a total count of 1 million were used for the positron lifetime experiments, which were carried out by a fast-slow coincidence ORTEC system with a time resolution of 230 ps full width at half-maximum. Positron lifetime calculations were performed using the ATSUP method,[26] in which the electron density and the positron crystalline Coulomb potential are constructed by the non-

dx.doi.org/10.1021/ja5085157 | J. Am. Chem. Soc. 2014, 136, 15670−15675

self-consistent superposition of free atom electron density and Coulomb potential in the absence of the positron.

Calculations. The first-principles calculations were carried out with the Vienna ab initio simulation package,[27] in which the generalized gradient approximation augmented by a Hubbard U term (GGA+U) with the PBE functional is used.[28] The energy cutoff was set to 400 eV, and the atomic positions were allowed to relax until the energy and force were less than 10^{-4} eV and 5×10^{-3} eV/Å, respectively. The on-site repulsion was treated within Dudarev's approach, where the on-site Coulomb repulsion (Hubbard U) and the atomic orbital intra-exchange energy (Hund's parameter J) are simplified to the single parameter U_{eff} ($U_{eff} = U - J = 2.0$ eV). The perfect (210)-oriented $CoSe_2$ nanosheets were simulated by periodically repeating the three CoSe layers along the [210] direction of the unit cell with a vacuum region of 15 Å, whereas the V_{Co}'' vacancy rich $CoSe_2$ nanosheets were simulated by removal of Co atoms from the surface of perfect (210)-oriented $CoSe_2$. The concentration of V_{Co}'' vacancies for the DFT calculations is 5%. The bulk $CoSe_2$ comparison was simulated by periodically repeating the 11 CoSe layers along the [210] direction of the unit cell.

Electrochemical Measurements. Electrocatalytic properties were studied with a standard three-electrode system controlled by a CHI660B electrochemical workstation. An Ag/AgCl (in 3 M KCl solution) electrode and a graphite rod (Alfa Aesar, 99.9995%) were used as the reference electrode and the counter electrode, respectively. To prepare the working electrode, 2 mg of catalyst and 30 μL of Nafion solution (5 wt %) were dispersed in 1 mL of ethanol−water mixed solvent with a volume ratio of 1:3 with sonication for at least 30 min to generate a homogeneous suspension. Then 5 μL of this solution (containing 20 μg of catalyst) was drop-casted onto a 3 mm diameter glassy-carbon electrode and then the solvent was evaporated at room temperature, yielding a catalyst loading of 0.142 mg cm^{-2}. All electrochemical measurements were conducted in 0.1 M KOH solution with a scan rate of 5 mV s^{-1}. The turnover frequency (TOF) was calculated on the basis of the reported methods,[29,30] and calculation details are given in the Supporting Information.

RESULTS AND DISCUSSION

The ultrathin $CoSe_2$ nanosheets were synthesized by an integrated process of liquid exfoliation and evaporation of the lamellar $CoSe_2$/DETA (DETA represents diethylenetriamine) intermediate (Supporting Information, Figure S1). The crystallinity of as-obtained ultrathin $CoSe_2$ nanosheets was determined by Raman spectra (Figure 2a), where the sharp peak at 190 cm^{-1} was assigned to the Se−Se stretching mode of cubic $CoSe_2$.[31] The XPS data in Figure 2b reveal the electron-binding energies of Co $2p_{3/2}$ at 778.3 eV and Co $2p_{5/2}$ at 793.4 eV, which are consistent with Co^{2+} cations in $CoSe_2$.[32] Meanwhile, an obvious satellite at the higher energy side of the Co 2p signal indicates the antibonding orbital between the Co atom and Se atom.[33] This result implies that the electronic structure of the obtained $CoSe_2$ corresponds to d^7 in the form of $t_{2g}^6 e_g^1$ near the optimal e_g filling of 1.2 for a high-activity paramagnetic configuration, which is desired for high-performance electrocatalysts. The TEM image in Figure 2c clearly reveals the 2D graphene-like morphology of the nanosheets, and its near-transparency indicates its ultrathin thickness. AFM images (Figure 2d) clearly show a smooth sheet with an average thickness of 1.4 nm. The X-ray diffraction pattern in Figure 2e clearly demonstrates a highly (210) preferred orientation in the ultrathin $CoSe_2$ nanosheet, which is consistent with the corresponding high-resolution TEM image (Figure 2f). Therefore, all of the results mentioned above clearly demonstrate that $CoSe_2$ ultrathin nanosheets were successfully fabricated.

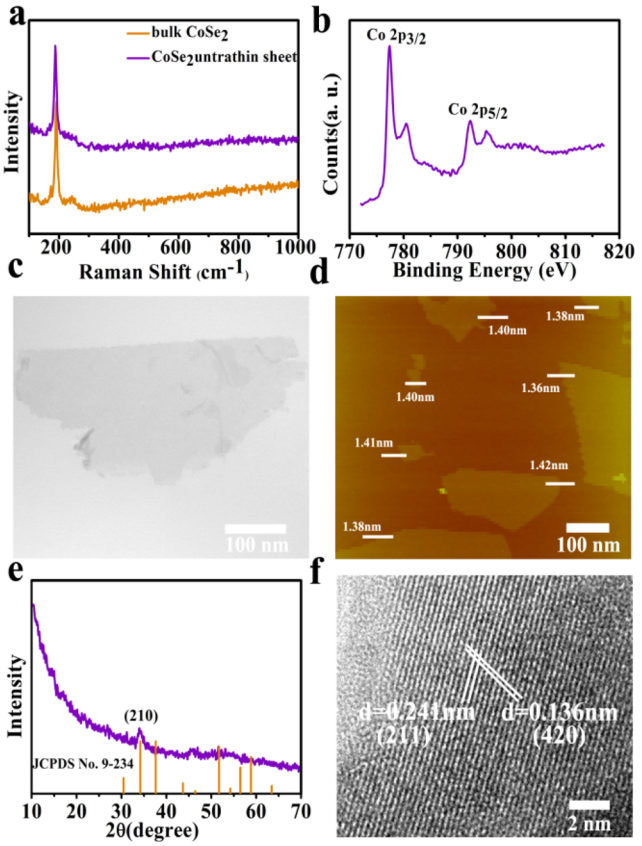

Figure 2. Characterization of $CoSe_2$ ultrathin nanosheets: (a) Raman spectra from bulk $CoSe_2$ and $CoSe_2$ ultrathin nanosheet; (b) XPS spectra of Co 2p; (c) TEM image; (d) AFM image; (e) XRD pattern for a $CoSe_2$ SLB film fabricated by LbL assembly; (f) HRTEM image.

In order to study the OER activity, electrochemical measurements of $CoSe_2$ ultrathin nanosheets as well as the bulk $CoSe_2$ were performed at a uniform loading of 0.142 mg cm^{-2} on a glassy-carbon (GC) electrode. The polarization curve for ultrathin $CoSe_2$ nanosheets in linear sweep voltammetry (LSV) curves exhibits higher current and earlier onset of catalytic current in comparison with those of the bulk $CoSe_2$ and $CoSe_2$/DETA (as shown in Figure 3a). It is simple and convenient to evaluate the electrocatalyst properties by comparing the overpotentials at the current density of 10 mA cm^{-2}. Remarkably, ultrathin $CoSe_2$ nanosheets can afford such current density at the small overpotential (η) of 0.32 V, significantly lower than 0.59 and 0.4 V for the bulk $CoSe_2$ and $CoSe_2$/DETA, respectively (Supporting Information, Figure S2). Moreover, ultrathin $CoSe_2$ nanosheets display the largest electrocatalytic reaction current, with 79.5 mA cm^{-2} at an overpotential of 500 mV, which is roughly 20 times larger than that of bulk $CoSe_2$. Since the electrocatalytic reaction current is directly proportional to the oxygen yield, the higher current density here indicates prominent oxygen evolution behavior in ultrathin $CoSe_2$ nanosheets. To obtain further insights into the oxygen evolution activity, Tafel plots of various catalysts were investigated. The resulting Tafel slope for the ultrathin $CoSe_2$ nanosheet is 44 mV/dec (Figure 3b), smaller than those of bulk $CoSe_2$ and $CoSe_2$/DETA, implying that the more rapid OER rate can be achieved in practical applications with ultrathin $CoSe_2$ nanosheets as electrocatalysts. To further assess the OER catalytic ability of the obtained nanosheets, we assumed that all of the Co ions are catalytically active and calculated

dx.doi.org/10.1021/ja5085157 | J. Am. Chem. Soc. 2014, 136, 15670−15675

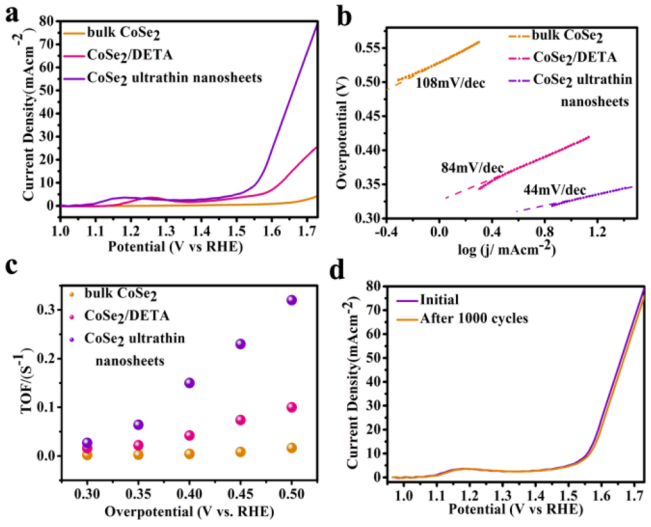

Figure 3. Water oxidation properties: (a) LSV curves and (b) corresponding Tafel plots in 0.1 M KOH medium with bulk $CoSe_2$, $CoSe_2$/DETA, and ultrathin $CoSe_2$ nanosheet as the electrocatalyst; (c) TOFs with respect to Co atoms of bulk $CoSe_2$, $CoSe_2$/DETA, and ultrathin $CoSe_2$ nanosheet at different overpotentials; (d) LSV curves obtained with as-prepared ultrathin $CoSe_2$ nanosheet before and after 1000 cycles of an accelerated stability test.

their turnover frequencies (TOFs) at different overpotentials, which were plotted against a function of overpotential. It is worth noting that these calculated TOFs represent the lowest limit, since some of these assumed metal sites are indeed inaccessible in the electrocatalysis reaction.[29,30] As shown in Figure 3c, the ultrathin $CoSe_2$ nanosheet shows much higher TOFs in comparison to those of both bulk $CoSe_2$ and $CoSe_2$/DETA. For example, at an overpotential of 0.5 V, the TOF of the ultrathin $CoSe_2$ nanosheet was 0.33 s^{-1}, more than 20 times higher than that of bulk $CoSe_2$ and larger in comparison to that of $CoSe_2$/DETA (Figure 3c and Supporting Information Table S2). Morever, the stability of the electrocatalyst is another important criterion for practical applications. To probe the durability of the ultrathin $CoSe_2$ nanosheet in an alkaline environment, continuous potential cycling was performed. As shown in Figure 3d, an imperceptible variation in the curves indicates the excellent stability of the ultrathin $CoSe_2$ nanosheets in a long-term electrochemical process. In addition, even after 1000 CV cycle catalytic tests, $CoSe_2$ still almost completely retained its morphology and structure (Supporting Information Figure S5), further verifying its excellent stability.

To gain a comprehensive understanding of the high OER activity within the ultrathin $CoSe_2$ nanosheet, local atomic arrangements and electronic structures of the sample were investigated. Since the positron annihilation spectrum (PAS) can provide direct information about the type and relative concentration of defects, it has become a strong technique to investigate defects in materials.[34,35] The positron lifetime spectra of both $CoSe_2$ ultrathin nanosheets and bulk $CoSe_2$ display three distinct lifetime components, τ_1, τ_2, and τ_3, with relative intensities I_1, I_2 and I_3 (Figure 4a and Table 1). The two longest components (τ_2 and τ_3) can be attributed to the large defect clusters and the interface presented in the material, respectively.[36] The shortest component (τ_1) could be assigned to positron annihilation as trapped V_{Co}'' vacancies. Moreover, we can gain further information about the relative concentration of the vacancy by the relative intensity (I) of the

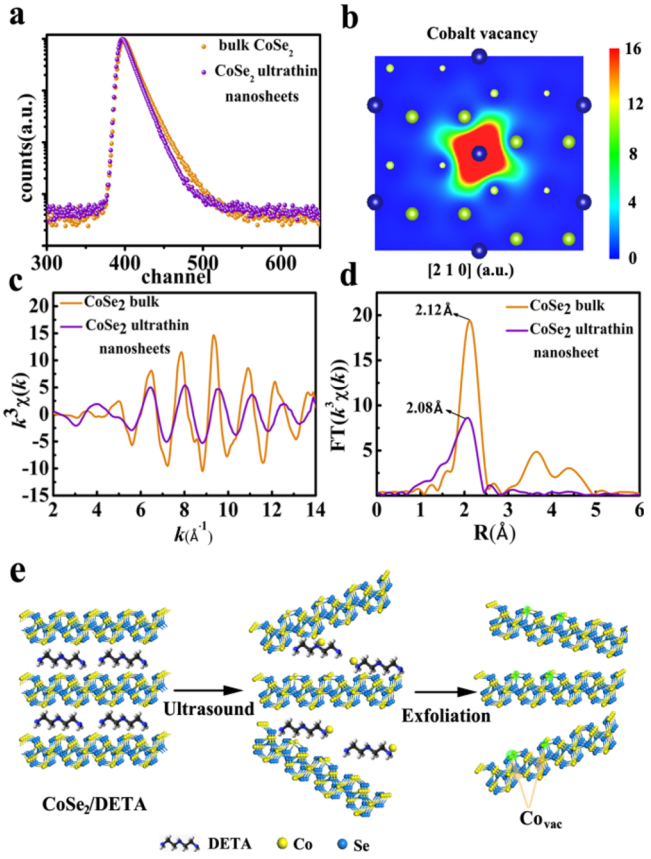

Figure 4. Positron lifetime spectra and XAFS measurements: (a) positron lifetime spectrum of ultrathin $CoSe_2$ nanosheets and bulk $CoSe_2$, respectively; (b) schematic representations of trapped positrons of cobalt vacancies; (c) Co K edge extended XAFS oscillation function $k^3[\chi(k)]$; (d) corresponding Fourier transforms (FT)$k^3[\chi(k)]$ (k = wave vector and $\chi(k)$ = oscillation as a function of photoelectron wavenumbe); (e) schematic of the formation of V_{Co}'' vacancies in $CoSe_2$ ultrathin nanosheets.

Table 1. Position Lifetime Parameters of Ultrathin $CoSe_2$ Nanosheets and Bulk

sample	τ_1 (ps)	τ_2 (ps)	τ_3 (ns)	I_1 (%)	I_2 (%)	I_3 (%)
nanosheet	216.1	417.0	1.79	73.0	26.8	0.2
bulk	208.9	459.8	1.60	16.5	83.2	0.3

positron. It is clear that V_{Co}'' vacancies and large defect clusters are predominant in ultrathin $CoSe_2$ nanosheets and bulk $CoSe_2$, respectively.

X-ray absorption fine structure spectroscopy (XAFS) measurements at the Co K edge were also performed. As shown in Figure 4c,d, the Co K-edge oscillation curve and corresponding Fourier transform (FT)$k^3[\chi(k)]$ functions in R space for the $CoSe_2$ ultrathin nanosheet display remarkable differences in comparison with that for the bulk counterpart, implying the different local atomic arrangements of the nanosheet (Supporting Information, Figure S6 and Table S1). The Fourier transformed curves of bulk $CoSe_2$ show the nearest Co−Se coordination with a main peak at 2.12 Å. In contrast, for the ultrathin $CoSe_2$ nanosheet, the peak intensities are decreased and shifted to low R by 0.04 Å. The weakened peak intensities can be attributed to surface structural disorder of the ultrathin nanosheet, and the coordination missing accompanied by V_{Co}'' vacancy formation. The low-R shift of the

dx.doi.org/10.1021/ja5085157 | J. Am. Chem. Soc. 2014, 136, 15670−15675

Co−Se peak is due to the significantly shortened Co−Se bond length that is exposed on the surface of the ultrathin nanosheet.

Combining the above PAS and XAFS characterizations above, we can unhesitatingly validate that V_{Co}'' vacancies are confined on the surface of the $CoSe_2$ ultrathin nanosheets. The underlying mechanism of V_{Co}'' vacancy formation is, in fact, closely related to the synthetic process (Figure 4e). Taking into account the structure of the lamellar hybrid intermediate $CoSe_2$/DETA, since the Co atoms and DETA are combined together by coordinate bonds, the ultrasonic treatment enables the DETA to drag the Co atoms detached from the lattice, resulting in the formation of the predominant V_{Co}'' vacancies for the ultrathin nanosheets.

In general, it has been proposed that H_2O molecules are initially adsorbed on the surface of catalysts during the electrocatalytic OER. That is to say, the adsorption energy of H_2O molecules plays a crucial role in the OER activity. We conducted a series of DFT calculations to study the H_2O adsorption on different cobalt sites of bulk $CoSe_2$ and ultrathin $CoSe_2$ nanosheets. Figure5a,b displays the binding energies

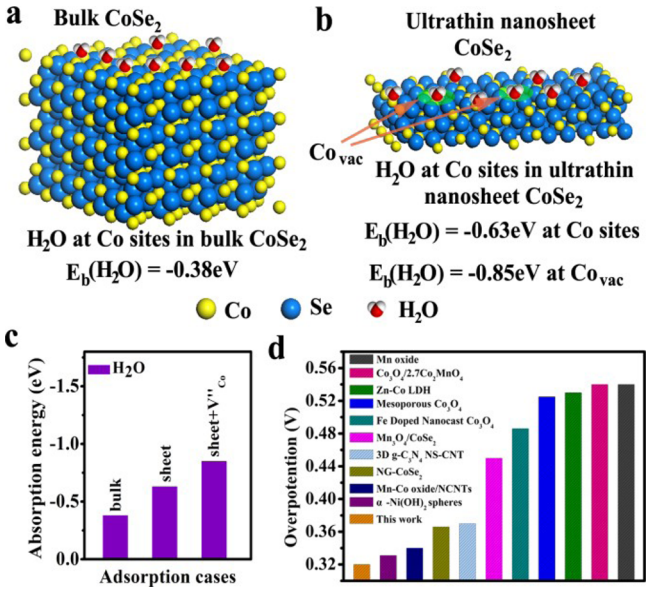

Figure 5. First-principles study of surface H_2O adsorption on different sites and performance of various materials: (a, b) geometries and binding energies of H_2O molecules on cobalt sites and vacancies; (c) calculated adsorption energies for H_2O molecules on different Co sites; (d) performance comparison under the same conditions of various materials, including Mn oxide,[37] Co_3O_4/2.7Co_2MnO_4,[38] Zn−Co LDH,[30] mesoporous Co_3O_4,[39] Fe-doped nanocast Co_3O_4,[40] Mn_3O_4/$CoSe_2$,[15] 3D g-C_3N_4 NS-CNT,[41] NG-$CoSe_2$,[16] spinel Mn−Co oxide/NCNTs,[42] and α-Ni(OH)$_2$ spheres.[43]

(E_b) of H_2O molecules on cobalt sites. It is clear that the surface cobalt sites and V_{Co}'' vacancy sites of ultrathin $CoSe_2$ nanosheets possess adsorption energies (absolute value) of 0.63 and 0.85 eV, respectively, obviously larger than that 0.38 eV of cobalt sites in bulk $CoSe_2$, indicating that the V_{Co}'' vacancies in the ultrathin structure were more favorable for adsorbing H_2O molecules. Accordingly, the ultrathin $CoSe_2$ nanosheet outperforms the bulk in intrinsic OER catalytic activity. The optimized electronic structures of ultrathin $CoSe_2$ nanosheets definitely determine their remarkably enhanced oxygen evolution activity. Moreover, the remarkably enhanced adsorption ability of H_2O molecules benefited from the V_{Co}'' vacancies as the thickness was reduced to atomic scale; the ultrathin $CoSe_2$ nanosheets also show OER activity much better than that of most reported Co-based electrocatalysts, indicating that ultrathin $CoSe_2$ nanosheets should be promising candidates to serve in the design of effective OER electrocatalysts and be more competitive in practical applications of sustainable energy technologies.

CONCLUSION

In conclusion, we successfully overcame the disadvantage of insufficient active sites in bulk $CoSe_2$ through reducing the thickness into the atomic scale. Our developed $CoSe_2$ ultrathin nanosheets with atomic thickness can effectively catalyze the oxygen evolution reaction with low overpotential, small Tafel slopes, and large turnover frequencies, which are all superior to those of its bulk counterparts and most reported Co-based electrocatalysts. Positron annihilation spectrometry, XAFS spectra, and first-principles calculations provide clear evidence that a number of V_{Co}'' vacancies are formed in the ultrathin $CoSe_2$ nanosheets, which can serve as active sites to effectively adsorb H_2O molecules, resulting in the significantly improved OER catalytic performance. Considering the outstanding performance for these simple, unmodified ultrathin $CoSe_2$ nanosheets as the only catalyst, further improvement of the catalytic activity is expected when various strategies of doping or hybridizing are used. These results not only demonstrate the potential of a notable, affordable, and earth-abundant water oxidation electrocatalyst based on ultrathin $CoSe_2$ nanosheets but also open up a promising avenue into the exploration of excellent active and durable catalysts that can replace noble metals for oxygen electrocatalysis.

ASSOCIATED CONTENT

Supporting Information

Figures, tables, and text giving characterization data for the $CoSe_2$/DETA hybrid and $CoSe_2$ bulk, TGA, FT-IR, elemental mapping, and stability for ultrathin $CoSe_2$ nanosheets, EXAFS curve-fitting and structural parameters of bulk $CoSe_2$ and ultrathin $CoSe_2$ nanosheets, OER parameters, and calculation details of TOF. This material is available free of charge via the Internet at http://pubs.acs.org.

AUTHOR INFORMATION

Corresponding Authors

*E-mail for C.X.: cxiao@ustc.edu.cn.
*E-mail for S.W.: sqwei@ustc.edu.cn.
*E-mail for Y.X.: yxie@ustc.edu.cn.

Author Contributions

‖These authors contributed equally to this reported research.

Notes

The authors declare no competing financial interest.

ACKNOWLEDGMENTS

This work was financially supported by the National Natural Science Foundation of China (11079004, 90922016, 11135008, 21331005, and 11321503), the innovation project of the Chinese Academy of Science (XDB01020300), the Fundamental Research Funds for the Central University (WK 2060190020), the China Postdoctoral Science Foundation (No. 2014M550347), and the Opening Project of the Jiangsu Key Laboratory for Environment Functional Materials (No. SJHG1301).

REFERENCES

(1) Lu, Y. C.; Xu, Z.; Gasteiger, H. A.; Chen, S.; Hamad-Schifferli, K.; Shao-Horn, Y. *J. Am. Chem. Soc.* **2010**, *132*, 12170.
(2) Cook, T. R.; Dogutan, D. K.; Reece, S. Y.; Surendranath, Y.; Teets, T. S.; Nocera, D. G. *Chem. Rev.* **2010**, *110*, 6474.
(3) Walter, M. G.; Warren, E. L.; McKone, J. R.; Boettcher, S. W.; Mi, Q.; Santori, E. A.; Lewis, N. S. *Chem. Rev.* **2010**, *110*, 6446.
(4) Gray, H. B. *Nat. Chem.* **2010**, *1*, 7.
(5) Kanan, M. W.; Nocera, D. G. *Science* **2008**, *321*, 1072.
(6) Zhao, Y.; Nakamura, R.; Kamiya, K.; Nakanishi, S.; Hashimoto, K. *Nat. Commun.* **2013**, *4*, 2390.
(7) Petrykin, V.; Macounova, K.; Shlyakhtin, O. A.; Krtil, P. *Angew. Chem., Int. Ed.* **2010**, *49*, 4813.
(8) Lee, Y.; Suntivich, J.; May, K. J.; Perry, E. E.; Shao-Horn, Y. *J. Phys. Chem. Lett.* **2012**, *3*, 399.
(9) Cheng, F. Y.; Shen, J.; Peng, B.; Pan, Y. D.; Tao, Z. J.; Chen, J. *Nat. Chem.* **2011**, *3*, 79.
(10) Liang, Y. Y.; Li, Y. G.; Wang, H. L.; Zhou, J. G.; Wang, J.; Regier, T.; Dai, H. J. *Nat. Mater.* **2011**, *10*, 780.
(11) Reece, S. Y.; Hamel, J. A.; Sung, K.; Jarvi, T. D.; Esswein, A. J.; Pijpers, J. J.; Nocera, D. G. *Science* **2011**, *334*, 645.
(12) Hurst, J. K. *Science* **2010**, *328*, 315.
(13) Subbaraman, R.; Tripkovic, D.; Chang, K. C.; Strmcnik, D.; Paulikas, A. P.; Hirunsit, P.; Chan, M.; Greeley, J.; Stamenkovic, N.; Markovic, N. M. *Nat. Mater.* **2012**, *11*, 550.
(14) Suntivich, J.; May, K. J.; Gasteiger, H. A.; Goodenough, J. B.; Shao-Horn, Y. *Science* **2011**, *334*, 1383.
(15) Gao, M. R.; Xu, Y. F.; Jiang, J.; Zheng, Y. R.; Yu, S. H. *J. Am. Chem. Soc.* **2012**, *134*, 2930.
(16) Gao, M. R.; Cao, X.; Gao, Q.; Xu, Y. F.; Zheng, Y. R.; Jiang, J.; Yu, S. H. *ACS Nano* **2014**, *8*, 3970.
(17) Zheng, Y. R.; Gao, M. R.; Gao, Q.; Li, H. H.; Xu, J.; Yu, S. H. *Small* **2014**, DOI: 10.1002/smll.201401423.
(18) Radisavljevic, B.; Radenovic, A.; Brivio, J.; Giacometti, V.; Kis, A. *Nat. Nanotechnol.* **2011**, *6*, 147.
(19) Sun, Y. F.; Liu, Q. H.; Gao, S.; Cheng, H.; Lei, F. C.; Sun, Z. H.; Jiang, Y.; Su, H. B.; Wei, S. Q.; Xie, Y. *Nat. Commun.* **2013**, *4*, 2899.
(20) Wu, C. Z.; Lu, X. L.; Peng, L. L.; Xu, K.; Peng, X.; Huang, J. L.; Huang, J. X.; Xie, Y. *Nat. Commun.* **2013**, *4*, 2431.
(21) Zhu, H. O.; Xiao, C.; Cheng, H.; Grote, F.; Zhang, X. D.; Yao, T.; Li, Z.; Cheng, H. M.; Wei, S. Q.; Xie, Y. *Nat. Commun.* **2014**, *5*, 3960.
(22) Zhu, Y. W.; Murali, S. T.; Stoller, M. D.; Ganesh, K. J.; Cai, W. W.; Ferreira, P. J.; Pirkle, A.; Wallace, R. M.; Cychosz, K. A.; Thommes, M.; Su, D.; Stach, E. A.; Ruoff, R. S. *Science* **2011**, *332*, 1537.
(23) Sun, Y. F.; Sun, Z. H.; Gao, S.; Cheng, H.; Liu, Q. H.; Piao, J. Y.; Yao, T.; Wu, C. Z.; Hu, S. L.; Wei, S. Q.; Xie, Y. *Nat. Commun.* **2012**, *3*, 1057.
(24) Guan, M. L.; Xiao, C.; Zhang, J.; Fan, S. J.; An, R.; Cheng, Q. M.; Xie, J. F.; Zhou, M.; Ye, B. J.; Xie, Y. *J. Am. Chem. Soc.* **2013**, *135*, 10411.
(25) Gao, M. R.; Yao, W. T.; Yao, H. B.; Yu, S. H. *J. Am. Chem. Soc.* **2009**, *131*, 7468.
(26) Robles, J. C.; Ogando, E.; Plazaola, F. *J. Phys.: Condens. Matter* **2007**, *19*, 176222.
(27) Kresse, G.; Furthmuller, J. *Comput. Mater. Sci.* **1996**, *6*, 15.
(28) Blochl, P. E. *Phys. Rev. B* **1994**, *50*, 17953.
(29) Gong, M.; Li, Y. Y.; Wang, H. L.; Liang, Y. Y.; Wu, J. Z.; Zhou, J. G.; Wang, J.; Regier, T.; Wei, F.; Dai, H. J. *J. Am. Chem. Soc.* **2013**, *135*, 8452.
(30) Zou, X. X.; Goswami, A.; Asefa, T. *J. Am. Chem. Soc.* **2013**, *135*, 17242.
(31) Kong, D. S.; Wang, H. T.; Lu, Z. Y.; Cui, Y. *J. Am. Chem. Soc.* **2014**, *136*, 4897.
(32) Lu, Q. Y.; Hu, J. Q.; Tang, K. B.; Deng, B.; Qian, Y. T.; Zhou, G. E.; Liu, X. M. *Mater. Chem. Phys.* **2001**, *69*, 278.
(33) Vanderheide, H.; Hemmel, R.; Vanbruggen, C. F. *J. Solid State Chem.* **1980**, *33*, 17.
(34) Xiao, C.; Qin, X. M.; Zhang, J.; An, R.; Xu, J.; Li, K.; Cao, B. X.; Yang, J. L.; Ye, B. J.; Xie, Y. *J. Am. Chem. Soc.* **2012**, *134*, 18460.
(35) Liu, X. W.; Zhou, K. B.; Wang, L.; Wang, B. Y.; Li, Y. D. *J. Am. Chem. Soc.* **2009**, *131*, 3140.
(36) Chakraverty, S.; Mitra, S.; Mandal, K.; Nambissan, P. M. G.; Chattopadhyay, S. *Phys. Rev. B* **2005**, *71*, 024115.
(37) Gorlin, Y.; Jaramillo, T. F. *J. Am. Chem. Soc.* **2010**, *132*, 13612.
(38) Wang, D. D.; Chen, X.; Evans, D. G.; Yang, W. S. *Nanoscale* **2013**, *5*, 5312.
(39) Tüysüz, H.; Hwang, Y. J.; Khan, S. B.; Asiri, A. M.; Yang, P. *Nano Res.* **2012**, *6*, 47.
(40) Grewe, T.; Deng, X. H.; Tüysüz, H. *Chem. Mater.* **2014**, *26*, 3162.
(41) Ma, T. Y.; Dai, S.; Jaroniec, M.; Qiao, S. Z. *Angew. Chem., Int. Ed.* **2004**, *57*, 7281.
(42) Zhao, A. Q.; Masa, J.; Xia, W.; Maljusch, A.; Willinger, M. G.; Clavel, G.; Xie, K. P.; Schlögl, R.; Schuhmann, W.; Muhler, M. *J. Am. Chem. Soc.* **2014**, *136*, 7551.
(43) Rao, M. R.; Sheng, W. C.; Zhuang, Z. B.; Fang, Q. R.; Gu, S.; Jiang, J.; Yan, Y. S. *J. Am. Chem. Soc.* **2014**, *136*, 7077.